Global NEST Journal, Vol 16, No 1, pp 80-86, 2014

SIMULATION OF THREE-DIMESIONAL OF COASTAL EROSION USING DIFFERENTIAL INTERFEROMETRIC SYNTHETIC APERTURE RADAR

MARGHANY M.

Institute for Science and Technology Geospatial (INSTeG)
Universiti Teknologi Malaysia
81310 UTM, Skudai, Johor Bahru, Malaysia

Received: 22/03/2013
Accepted: 02/10/2013
*to whom all correspondence should be addressed:
e-mail: maged@utm.my; magedupm@hotmail.com

ABSTRACT

This study aims at modelling three-dimensional shoreline change rates using differential interferometric synthetic aperture radar (DInSAR) techinuqe. Neverthless, decorrelation plays significant role to control the accuracy of three dimensional object reconstruction using DInSAR. To solve this problem, multichannel MAP height estimator algorithm is implemented with in ENVISAT ASAR data. Therefore, the proposed method has been applied to coastaline of Johor, Malaysia. The study shows the critical erosion of -3.5 m y^{-1} with accuracy (RMSE) of ±0.05 m. In addition, the volume rate of shoreline changes of -2343.42 m^3 y^{-1} corresponds to the lowest digital elevation model (DEM) of 7.4 m. It can be said that accurate rate of shoreline change can be achieved with root mean square error (RMSE) of ±0.05 m using multichannel MAP height estimator algorithm.

KEYWORDS: DInSAR,ENVISAT ASAR, Coastal erosion, multichannel MAP height estimator algorithm.

1 INTRODUCTION

Both natural and man-made disasters are the main factors for coastal hazards which occur along the coastline. Both factors can cause tremendous damage to coastline geomorphology features and infrastructures. Natural hazards, therefore, are disasters which are out of mankind control and regularly occurred by weather fluctuations. For instance, storms, tsunamis, typhoons, flooding, tides, waterspouts, nor'easters, and storm surge are major significant disasters which can damage coastal zone geomorphological features and human life. Besides, human can cause permanent disasters in the coastal zone through pollution, trawling, and human rapid development. All together, both catastrophes resume to harm the marine ecosystem cruelly and they request to be investigated for possible control and end. As a result, coastal erosion is one of critical catastrophes which can be caused by nature and human activities.

According to Marghany *et al.* (2010; 2011) and Marghany (2001), conventional methods for coastal erosion studies are required to be updated to standard and accurate methods. Recently, interferometric synthetic aperture radar (InSAR) techniques have provided excellent promised for detection of sub-millimeter of the Earth surface deformation (Guariglia *et al.*, 2006). Scientists have implemented the InSAR technique for investigation of volcano dynamics, co-seismic and post-seismic motion, urban subsidence along with landslides (Gens and Genderen, 1996; Zebker *et al.,* 1997; Massonnet and Feigl, 1998; Gens, 2000; Luo *et al.*, 2006). Yet, InSAR technique does not use extensively in the estimation of the shoreline rate of changes. Consequently, there are few efforts were done by Hangdog *et al.*, (2011); Marghany (2012) and (2013) using differential interferometric synthetic aperture radar (DInSAR) for digital elevation model (DEM) of the coastal geomorphology spit of the small scale area of 300 m x 500 m. Nevertheless, there are several factors can effectively impact the accuracy of DEM from InSAR technique. According to Aiazzi *et al.* (2005), the phase estimation is a major challenge to determine more accurate DEM. This is because of the measured phase differences are given as a wrapped phase field of the principal values of a range –π to π, thus the existence unspecified within multiples of 2 π (Nizalapur *et al.,* 2011). This procedure produces

phase jumps between neighboring pixels. Smooth function is used to resolve phase jump by adding or subtracting multiples of 2 π (Sumantyo *et al.,* 2012). Consequently, multichannel MAP height estimator based on a Gaussian Markov Random (GMRF) has developed by Ferretti *et al.* (2001), Ferraiuolo *et al.* (2004), Baseline *et al.* (2009), Ferraiuolo *et al.* (2009) to solve the uncertainties of DEM reconstruction from InSAR technique. They found that the multichannel MAP height estimator has managed the phase discontinuities and improved the DEM profile. Recently, Marghany (2012) validated GMRF technique with a lower range of error (0.01±0.11 m) with 90% confidence intervals for DEM reconstruction using RADARSAT-1 SAR F1 mode data.

We hypothesized that shoreline erosion can be investigated as surface deformation or displacement. In this regard, multichannel MAP height estimator algorithm with phase unwrapping can produce accurately digital elevation model (DEM) of shoreline deformation. In doing so, this study extends the previous work was done by Baseline *et al.* (2009), Ferraiuolo *et al.* (2009) and Marghany (2012) by implementing a GMRF technique with InSAR procedures. Further, it uses three C-band SAR images acquired by an ASAR sensor on board satellite ENVISAT simulate three-dimensional (3-D) shoreline rate of changes.

2. METHODS

2.1 Data Set

SAR data acquired in this study were derived from ENVISAT images from an Advanced Synthetic Aperture Radar (ASAR) sensors and operates in the C band in a wide variety of modes. It can detect changes in surface heights with sub-millimeter precision. These data are C-band and had the lower signal-to-noise ratio owing to their VV polarization with a wavelength range of 3.7 to 7.5 cm and a frequency of 5.331 GHz (Table 1). ASAR can achieve a spatial resolution generally around 30 m.

Table 1. ENVISAT ASAR characteristics were used in this study

Parameters	Values
Radar Wavelength (cm)	5,6
Orbit Repeat Time, days	14 11/35
Pulse Repetition (PRF), Hz	1316.000000
Ground Resolution	30
Swath Width (km)	105
Incident Angle (°)	19.2-26.7
Polarization	HH/VV

The ASAR is intended for applications which require the spatial resolution of spatial resolution of 150 m. This means that it is not effective at imaging areas in depth, unlike strip map SAR (ESA 2013). The azimuth resolution is 4 m, and range resolution ranges between 8 m (Table 1).

2.2 MULTICHANAL MAP

Following Marghany (2012), the important dimension in DInSAR is the component of the shoreline geomorphology changes in the slant range direction. According to Massonnet and Feigl (1998) the shoreline deformation is therefore given by

$$|m| = \frac{\lambda \Delta\phi}{2\pi \sin(\theta_i - \zeta)} \quad (1)$$

where m the coastline deformation vectors that is describing the direction and magnitude of the surface changes, θ_i is the ENVISAT ASAR data incident angle, ζ the shoreline 's elevation, and the phase difference $\Delta\phi$ between the two ENVISAT ASAR data positions and the pixel of target of terrain point is given by the adapted equation of Zebker *et al.* (1994)

$$\Delta\zeta = \frac{\lambda R \sin\theta}{4\pi B} \Delta\phi \quad (2)$$

Equation 2 is a function of normal base line B, and the range R . In addition, equation 2 can provide information about the heights and phase differences estimations. In fact, the estimated height of each pixel of ENVISAT ASAR data is an important task to generate a raster form of the DEM.

Under this circumstance, Marghany (2012) recommended to use the multichannel MAP height estimator used to reconstruct the fringe pattern, and 3-D from decorrelate unwrapped phase. Following Ferraiuolo *et at*. (2009) and Marghany (2012) a MAP height estimation can be given by

$$\hat{\varsigma}_{MAP} = \arg_{\varsigma} \max \ln \left[\left(\prod_{S=1}^{S} F_{mc}(\phi_s \left| \varsigma_s \right.) g(\varsigma; \hat{\sigma}) \right] \right. \quad (3)$$

where $g(.)$ is a prior probability density function (pdf) which is adopted by using Gaussian Markov Random Field and $\hat{\sigma}$ is the hyperparmeter vector which is not a prior known. According to Baselice *et al.* (2009) , it has to be estimated starting from the measured interfergrams. This is accomplished by considering sub-bands, corresponding to different azimuth looks. In this context, a Gaussian Markov Random Field (GMRF) as a-priori model, whose expression is:

$$g(\varsigma, \hat{\sigma}) = \frac{1}{Z(\sigma)} e^{(-\sum_{S=1}^{SxN} \sum_{K \in N_S} \left[\frac{(\varsigma_s - \varsigma_k)^2}{2\sigma_{sk}^2} \right]} \quad (4)$$

where ς is height, N_s is the neighborhood system of s^{th} pixel, and s are the so-called hyperparameters, which are representative of the local characteristics of the image h, σ is the hyperparameter vector collecting all s values, and $Z(\sigma)$ is the partition function necessary to normalize the pdf (Marghany 2012). Although the reconstruction, considering the limited number of available data (four channels), is good, we want to improve its quality, particularly on the discontinuities. Then, the algorithm is implemented based on the ground elevation data collections.

Then the shoreline deformation rate $\hat{\varsigma}_{MAP}$ is estimated using equation 3. Finally, the accuracy assessment is estimated root mean square error (RMSE) using the following formula

$$RMSE = \frac{\sqrt{(\hat{\varsigma}_{MAP} - \varsigma_g)^2}}{N-1} \quad (5)$$

where $\hat{\varsigma}_{MAP}$ is coastal deformation retrieved using GMRF algorithm and ς_g is ground data that collected during satellite overpasses and *N* is the number of samples which are 200 sample points to indemnify the precise accuracy of DInSAT technique.

3 RESULTS AND DISCUSSION

In the present study, DInSAR methods are implemented on ENVISAT ASAR data sets of 5 March 2003 (SLC-1), 28 April 2003 (SLC-2) and January 25, 2011, (SLC-3) of Wide Swath Mode (WSM) (Figure 1). They are acquired from ascending (Track: 226, orbit: 5290), descending (Track: 490, Orbit: 6055) and descending (Track 420,Orbit 4655), respectively. These data have acquired over the coastline of Johor in the southern eastern part of Peninsular Malaysia. The area is approximately 20 km of Johor (Figure 1a), located in the South China Sea between 1° 57′ N to 2° 15′ N and 103° 51′ E to 104° 15′ E.

Figure 2a and Figure 2b present the reference DEM which has been generated from topographical 1:50000, and ground measurements, respectively while Figure 2c shows the ENVISAT coherence data. It is clear that the maximum elevation of 50 m which found in land. The maximum elevation of 10 m is shown along the coastline. The high coherence rates are existed in urban zone and along infrastructures with 0.9 while low coherence of 0.2 is found in a vegetation zone along the coastline.

According to Nizalapur *et al.* (2011), heavy vegetation covers can cause poor coherence and can lead to decorrelation. Since three ASAR data acquired in the wet northeast monsoon period, there has been an impact of wet sand on a radar signal penetration which causing weak penetration of radar signal because of dielectric. This agrees with the work of Zebker *et al.* (1994) and Zebker *et al.* (1997). Indeed, the total topographic decorrelation effects along the radar-facing slopes are dominant and highlighted as lowest coherence value of 0.2. According to Marghany (2013) the micro-scale movement of the sand particles driven by the coastal hydrodynamic, and wind speed of

12 m s^{-1} could change the distribution of scatters resulting in rapid temporal decorrelation which has contributed to lowest coherence along coastline. This result agreed with Marghany (2012).

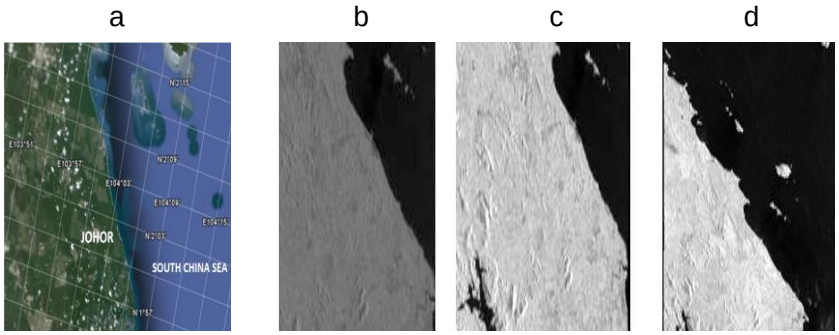

Figure 1. ENVISAT ASAR data used in this study over (a) coastline of Johor and during (b) 5 March 2003; (c) 28 April 2003; and (d) January 25 2011

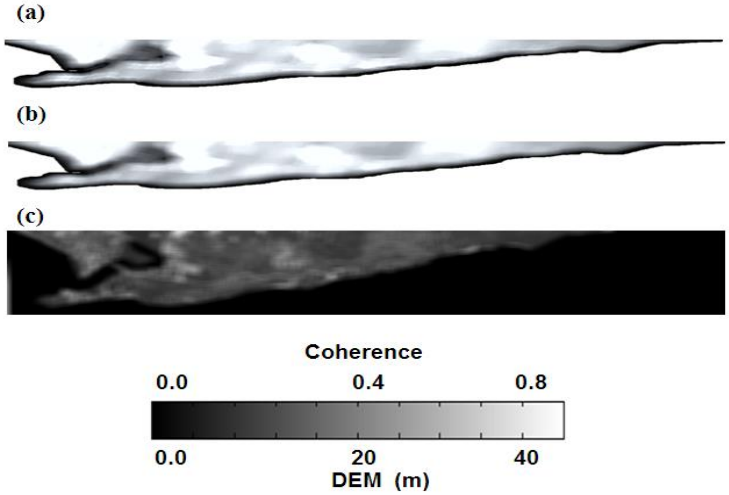

Figure 2. DEM generated from (a) topographic map; (b) in situ measurements; and (c) coherence ENVISAT ASAR

Figure 3 shows the interferormetry constructed using the multichannel MAP height estimator. The module 2 π is presented the phase difference which its color encoded in the fringes. Figure 3 illustrates the full color cycle that represents a phase cycle, and covering a range between –π to π. Apparently, the color bands change in the reverse order, indicating that the center has a great deformation along the shoreline. This shift corresponds to -1.5 m y^{-1} of coastal deformation over the distance of 10000 m. Multichannel MAP height estimator produced a precise pattern of fringe interfeormetry (Figure 4). It shows there are many deformations of over several centimeters. In these deformations, it is known the deformation in shoreline because of sedimentation transport. Further, it can be noticed that Multichannel MAP height estimator detailed edges with discernible fringes. Indeed, Figure 3 Shows smooth interferormetry pattern, in terms of spatial resolution maintenance, and noise reduction, compared to conventional methods. This result validates the study of Marghany (2012).

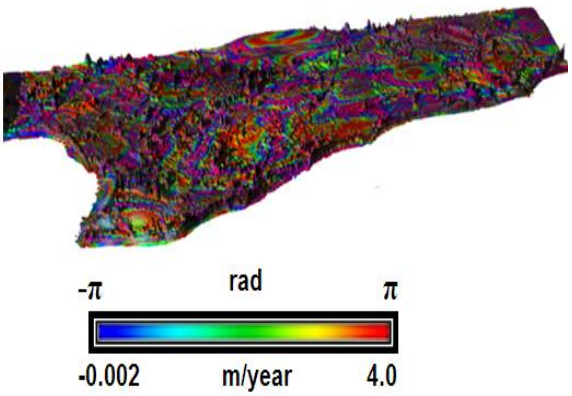

Figure 3. Fringe interferometry generated by a the multichannel MAP height estimator algorithm

Figure 4 represents a 3-D shoreline reconstruction using the multichannel MAP height estimator with the maximum shoreline 's elevation is 10.5 m with sharp slope of 3 m. It is interesting to find that the lowest DEM of 7.4 m coincides with the volume rate of changes of -2343.42 m^3 y^{-1}. This is indicating critical erosion of -3.5 m y^{-1} (Figure 2). According to Marghany (2012), the northeast monsoon period can cause significant erosion because of highest wave energy input in Malaysian coastal waters.

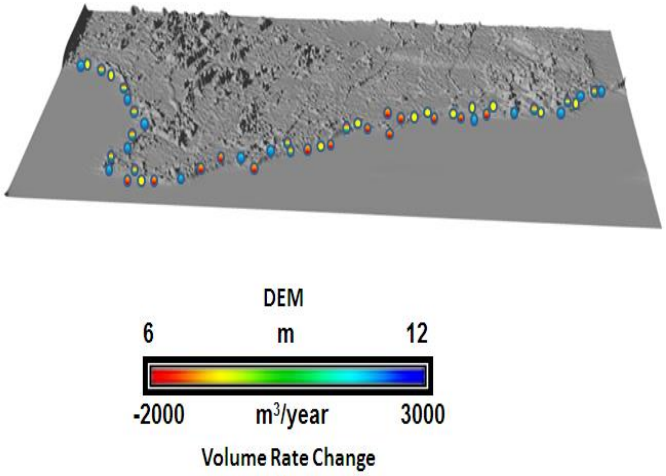

Figure 4. 3-D of shoreline volume change rate generated multichannel MAP height estimator algorithm

According to Marghany (2013), the geological structure of the shoreline composed of alluvium soil, and carbonate rock with the decaying living organism. This can escalate the coastal erosion rate as these sediments are washed from the shoreline by strong wave energy. Evidently, Figure 5 shows excellent correlation between shoreline change rates modelled using multichannel Map height and ground measurements. The scatter points in Figure 5 are closer to the regression line with a coefficient of determination r^2 of 0.83, the probability p of 0.004, and accuracy (RMSE) of ±0.05 m which is relatively higher than work was done by Yang *et al.* (2007) and Marghany (2013). Indeed, Marghany (2013) has implemented fuzzy B-spline algorithm with phase unwrapping but Yang *et al.* (2007) used a fuzzy algorithm as a filter for unwrapping phase.

In addition to different algorithms, Marghany (2012) and (2013) studied DInSAR technique with the small scale area of 300 m^2. According Baselice *et al.* (2009) and Marghany (2012), the local estimation of hyperparameters allows one to localize the flat regions and the discontinuities of the image, in view of the local characteristics of the profile and producing a hyperparameter map for the profile. This leads to a powerful and general model, well suited to represent a wide class of height profiles (Figure 3). Further, Marghany (2012) stated that Gaussian Markov Random Field (GMRF) can correct fringe discontinuities, and provides a large number of interpolated samples over

corrupted fringe detail. This work confirms the study of Ferretti *et al.* (2001), Ferraiuolo *et al.* (2004), Baseline *et al.* (2009), Ferraiuolo *et al.* (2009), and Marghany (2012). These suggest that a multichannel MAP height estimator algorithm is an excellent method to 3-D shoreline change rate simulation that is based on DInSAR technique.

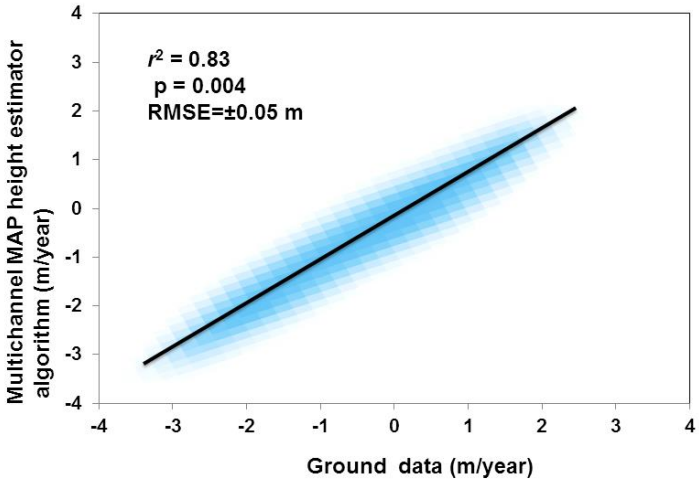

Figure 5. Regression model between ground data and multichannel MAP height estimator algorithm

CONCLUSIONS

This study demonstrated a method to simulate three-dimensional shoreline change rates using DInSAR technique. Using the proposed multichannel MAP height estimator algorithm is implemented in ENVISAT ASAR data that acquired in different periods. The study shows that the lowest DEM of 7.4 m coincides with the volume rate of changes of -2343.42 m^3 y^{-1} and critical erosion of -3.5 m y^{-1}. In conclusion, multichannel MAP height estimator algorithm is an excellent method for 3-D coastal erosion mapping with accuracy (RMSE) of ±0.05 m.

REFERENCES

Aiazzi B., Baronti S., Bianchini M., Mori A. and Alparone L. (2005), Filtering of interferometric SAR phase images as fuzzy matching-pursuit blind estimation, *EURASIP Journal on Applied Signal Processing*, **20**, 3220-3230.

Baselice F., Ferraioli, G. and Pascazio,V. (2009), DEM reconstruction in layover areas from SAR and auxiliary input data, *IEEE Geoscience Remote Sensing Letters*, **6**, 253-257.

ESA (2013), What is ENVISAT [https://earth.esa.int/web/guest/missions/esa-operational-eo-missions/envisat] [Access on March 13 2013].

Ferraiuolo G., Meglio F., Pascazio V. and Schirinzi G. (2009), DEM Reconstruction Accuracy in Multichannel SAR Interferometry, *IEEE Transactions in Geoscience and Remote Sensing,* **47**, 191-201.

Ferraiuolo G., Pascazio V. and Schirinzi G. (2004), Maximum a posteriori estimation of height profiles in InSAR imaging, *IEEE Geoscience Remote Sensing Letters*, **2**, 66-70.

Ferretti A., Prati C. and Rocca F. (2001), Multibaseline phase unwrapping for InSAR topography Estimation, *Il Nuovo cimento della Società italiana di fisica. C. Geophysics and space physics*, **24**, 159-176.

Gens R. and van Genderen J.L. (1996), Review Article: SAR Interferometry: issues, techniques, applications, *International Journal of Remote Sensing,* **17**,1803-1835.

Gens R. (2000), The influence of input parameters on SAR interferometric processing and its implication on the calibration of SAR interferometric data, *International Journal of Remote Sensing,* **2**, 11767–1771.

Guariglia A., Buonamassa A., Losurdo A., Saladino R., Trivigno, M.L., Zaccagnino A. and Colangelo A. (2006), A multisource approach for coastline mapping and identification of shoreline changes, *Annals of Geophysics*, **49**, 295-304.

Hangdog F., Kazhong D., Chengyu J., Chuanguang Z., Jiqun X., (2011) Land subsidence monitoring by D-InSAR technique, *Mining Science and Technology (China)*, **21**, 869–872.

Luo X., Huang F. and Liu G. (2006), Extraction co-seismic Deformation of Bam earthquake with Differential SAR Interferometry", *Journal New Zealand. Institute of Survy*, **296**, 20-23.

Marghany M. (2012a),Three dimensional Coastal geomorphology deformation modelling using differential synthetic aperture interferometry, *Verlag Der Zeitschrift fur Naturforschung*, **67a**, 419-420.

Marghany M. (2012b), DEM reconstruction of coastal geomorphology from DInSAR: In Murgante B. *et al.* (eds.), *Lecture Notes in Computer Science (ICCSA 2012)*, Part III, LNCS, **7335**, 435–446.

Marghany M. (2013), DInSAR technique for three-dimensional coastal spit simulation from Radarsat-1 fine mode data, *Acta Geophysica*, **61**, 478-493.

Marghany M., (2001), TOPSAR wave spectra model and coastal erosion detection, *International Journal of Applied Earth Observation and Geoinformation*, **3**, 357-365.

Marghany M., and Hashim M. (2010), Different polarised topographic synthetic aperture radar (TOPSAR) bands for shoreline change mapping, *International Journal of Physical Science, **5***, 1883-1889.

Marghany M., Hashim M., and Cracknell A.P. (2011),Simulation of shoreline change using AIRSAR and POLSAR C-band data, *Environmental Earth Sciences*, **64,** 1177–1189.

Massonnet D. and Feigl K.L., (1998), Radar interferometry and its application to changes in the earth's surface, *Review Geophysics,* **36**, 441–500.

Nizalapur V., Madugundu R. and Shekhar C.J. (2011), Coherence-based land cover classification in forested areas of Chattisgarh, Central India, using environmental satellite—advanced synthetic aperture radar data, *Journal of Applied Remote Sensing,* **5**, 059501-1-059501-6.

Sumantyo J.T.S., Shimada M., Mathieu P., Abidin H.Z. (2012), Long-term consecutive DInSAR for volume change estimation of land deformation, *IEEE Transactions on Geoscience* and Remote Sensing*,* **50**, 259 – 270.

Yang J., Xiong T. and Peng Y. (2007), A fuzzy approach to filtering interferometric SAR data: *International Journal of Remote Sensing,* **28**, 1375-1382.

Zebker H.A., Rosen P.A. and Hensley S. (1997), Atmospheric effects in interferometric synthetic aperture radar surface deformation and topographic maps: *Journal of Geophysical, Research,* **102**, 7547–7563.

Zebker H.A., Werner C.L., Rosen P.A. and Hensley S. (1994), Accuracy of topographic maps derived from ERS-1 interferometric radar, *IEEE Transactions on Geoscience and Remote Sensing,* **2**, 823-836.